Injection Kinetics and Electronic Structure at the N719/TiO_2 Interface Studied by Means of Ultrafast XUV Photoemission Spectroscopy

Mario Borgwardt,[†] Martin Wilke,[†] Thorsten Kampen,[‡] Sven Mähl,[‡] Wanchun Xiang,[¶] Leone Spiccia,[¶] Kathrin M. Lange,[‖] Igor Yu. Kiyan,[†] and Emad F. Aziz[*,†,⊥]

†*Joint Laboratory for Ultrafast Dynamics in Solutions and at Interfaces (JULiq), Institute of Methods for Material Development, Helmholtz-Zentrum Berlin, Albert-Einstein-Strasse 15, D-12489 Berlin, Germany*

‡*SPECS Surface Nano Analysis GmbH, Voltastrasse 5, D-13355 Berlin, Germany*

¶*School of Chemistry and ARC Centre of Excellence for Electromaterials Science (ACES), Monash University, Clayton 3800, VIC, Australia*

§*State Key Laboratory of Silicate Materials for Architectures, Wuhan University of Technology, Hubei, 430070, China*

‖*Institute of Solar Fuels, Helmholtz-Zentrum Berlin, Albert-Einstein-Strasse 15, D-12489 Berlin, Germany*

⊥*Department of Physics, Freie Universität Berlin, Arnimallee 14, 14195 Berlin,Germany*

E-mail: emad.aziz@helmholtz-berlin.de

Abstract

The method of transient XUV photoemission spectroscopy is developed to investigate the ultrafast dynamics of heterogeneous electron transfer at the interface between the N719 ruthenium dye complex and TiO_2 nanoparticles. XUV light from high-order harmonic generation is used to probe the electron density distribution among the ground and excited states at the interface after its exposure to a pump laser pulse of 530 nm wavelength. A spectral decomposition of the transient emission signal is used to follow the population and decay dynamics of the involved transient states individually. By comparing results obtained for the N719/TiO_2 and N719/FTO interfaces, we can unambiguously reveal the kinetics of electrons injected to TiO_2 from the singlet metal-to-ligand charge-transfer (MLCT) excited state of the dye. With the developed approach, we characterize both the kinetic constants and the absolute binding energies of the singlet and triplet MLCT states of the dye and the state of electrons injected to the conduction band of TiO_2. The energy levels of the singlet and triplet states are found to lie 0.7 eV above and 0.2 eV below the conduction band minimum, respectively. This energetic structure gives rise to a strong driving force for injection from the singlet state and a slow electron transfer from the triplet state, the latter being possible due to a partial overlap of the triplet state band of N719 and the conduction band of TiO_2.

Introduction

Heterogeneous electron transfer (HET) at the interface between a dye and a wide-band-gap semiconductor has attracted much interest in the last decades.[1] Following the invention of nanostructured dye-sensitized solar cell by Grätzel and O'Regan,[2] considerable efforts have been made to investigate fundamental processes induced by light in this devices. Among various combinations of the sensitizer and semiconductor materials, the ruthenium-based dye complexes, such as $Ru(dcbpyH)_2(NCS)_2$ (N3) and its salt $(Bu_4N)_2Ru(dcbpyH)_2(NCS)_2$ (N719), exhibit high efficiency (close to unity) of the HET mechanism in the visible range

of the solar spectrum.[3–5] Due to this property and the achievement of solar-to-electric energy conversion efficiency exceeding 10%, the N719 complex has been considered over the years as a reference dye for studying fundamental aspects of photo-induced electron transfer properties in the DSSCs.[4,6] The high injection yield of electrons into the semiconductor state is related to a rather fast HET process compared to other competing reaction channels. In order to reveal the competition of different processes, the application of ultrafast time-resolved spectroscopies is, therefore, needed to follow the complex electron dynamics induced by photoexcitation at the dye-semiconductor interface.

Femtosecond transient absorption spectroscopy represents so far the most common method used for studying the electron dynamics at interfaces. This method was applied, in particular, to investigate the injection kinetics from the Ru-based dye complexes to a TiO_2 layer. The injection process was found to exhibit a coexistence of an ultrafast (≤ 100 fs) transfer component and one or more slower components occurring on a picosecond and even longer timescales.[7–11] This feature is associated with the population dynamics of different metal-to-ligand charge-transfer (MLCT) states of the dye complex. Following excitation at the maximum of the absorption band (typically at a wavelength of 530 nm), the dye is initially prepared in the singlet ^{1}MLCT state. This state promotes the fast electron transfer directly into the conduction band (CB) of TiO_2, which takes place simultaneously with an internal relaxation into the triplet ^{3}MLCT state via intersystem crossing.[12–15] Both injection and relaxation processes were found to occur on a timescale of $50 - 100$ fs.[16,17] Injection from the relaxed triplet state is significantly slower and occurs on a picosecond time scale. To account for the competition in the injection kinetics between the direct electron injection and the intramolecular relaxation, Asbury *et al.*[15] proposed a two-state injection model. The ratio between the short- and long-lived states were found to depend on the excitation wavelength, confirming that the main injection channel originates from the non-thermalized singlet ^{1}MLCT state.[15]

Apart from the injection kinetics, the binding energies of the ground and excited states

and their match at the dye–semiconductor interface are fundamentally important for the function of a DSSC. On the one hand, the energy difference between the donor (excited dye) and the acceptor (CB of TiO_2) determines the driving force for the electron transfer,[18] and on the other hand the excess energy represents a dissipation mechanism and by that influences the overall reachable conversion efficiency of the cell. Thus, a detailed knowledge of the energy structure is inevitable to better understand various experimental aspects and to specifically design new and more efficient sensitizers. For Ru-based sensitizers, the ground- and excited-state redox potentials were measured by cyclic voltammetry combined with absorption and emission spectroscopy.[19–21] The molecular band alignment with the CB of TiO_2 was predicted by theory and the calculated results were verified by comparison with the absorption spectra.[22,23] However, direct experimental knowledge of the energetics at the dye-semiconductor interface is not available until today and the development of other approaches is required to gain insight into the actual band alignment.

The method of transient absorption spectroscopy does not provide a direct measure of binding energies. The changes in absorption signal are related to the formation of positively charged dye cations or to the density increase of free electrons in the CB of the semiconductor. The actual transitions that involve population of excites states are probed indirectly and it is difficult to draw conclusions about the energy structure in this case. In the present work we apply femtosecond time-resolved photoemission spectroscopy (PES) and demonstrate the capabilities of this method in both revealing the injection kinetics and determining the binding energies of the involved states. In a transient PES experiment, a short laser pulse in the visible wavelength range excites the dye to a higher-lying state, whereas as a second short pulse of high photon energy is applied at a variable time delay to ionize the system. To be able to probe the ground and the excited states simultaneously, the photon energy of the probe pulse needs to be sufficiently high (> 7 eV). Tabletop XUV light sources generating pulses of ultrashort duration and employing up-conversion of the fundamental laser frequency via the process of high-order harmonic generation (HHG) in a non-linear

medium, nowadays represent a well understood and established technique.[24,25] With the use of modern femtosecond pump lasers, this technique allows the generation of a high photon flux in the XUV energy range reaching $\sim$ 100 eV and finds its application in a variety of different research fields.[26–29]

In the present work, we employ our recently developed HHG setup dedicated to time-resolved PES studies.[30] We confirm the current understanding of ultrafast charge transfer at the N719/TiO_2 interface and provide additional information about the binding energies for the involved excited states. As a reference sample, we use the fluorine-doped SnO_2 substrate (FTO) covered with dye to ensure sufficient conductivity thereby avoiding charging effects. By measuring the injection kinetics at the N719/TiO_2 interface in comparison to the N719/FTO interface, we can clearly distinguish the unique properties of the TiO_2 electrode. Such a comparison is straightforward to make, since the HET process at the N719/FTO interface is much slower and, in particular, the ultrafast injection component is highly suppressed.[31,32]

Experimental section

Sample preparation

The glass substrate of 4 mm thickness, coated with a conductive FTO layer of 10 Ω/cm^2 resistivity, was purchased from Nippon Sheet Glass (NSG, Japan). An area of 4×4 mm^2 size on the FTO layer surface was coated with a mesoporous TiO_2 film with the use of a commercial semi-automatic screen printer and a commercial printing paste containing colloidal TiO_2 particles of 18 nm average size (PST-18 NR, JGC Catalysts and Chemicals). The N719 dye was purchased from Dyesol (Australia). For sensitization, a solution was prepared with a 0.3 mM dye concentration in a mixture of acetonitrile and tert-butylalcohol with a volume ratio of 1:1. Prior to sensitization, the TiO_2 film was sintered at 500 °C for 30 minutes. After the substrate was cooled to 80 °C, the TiO_2 electrode was immersed into

the dye solution and kept at room temperature for 24 hours. The films were rinsed by the same solvent mixture to remove unbound dye and afterward were transferred in atmosphere into the experimental vacuum chamber. A typical residual gas pressure in the chamber was in the range of 10^{-7} mbar during experiment. The absorbance of the dye-sensitized film was 0.24 at the wavelength of 530 nm, as measured with a home-built UV/visible absorption spectrometer.

The part of the FTO layer surface which remained uncoated with TiO_2 served as a reference sample, with the dye not linked to TiO_2. After immersion of the substrate in the dye solution, both the TiO_2 film and the free part of the FTO layer were covered with dye, giving rise to the N719/TiO_2 and N719/FTO interfaces, respectively. In addition, electron emission was measured from bare TiO_2 and FTO layers (denoted below by bTiO_2 and bFTO, respectively) so that four samples were investigated in total.

The samples were prepared immediately prior to measurements. No degradation or modification of sample was observed in the steady-state XUV spectra recorded before and after the pump-probe measurements. Because of the ex-situ sample preparation, special attention was paid to possible surface contamination, e.g., by water or organic materials, which may influence binding energies as well as the injection kinetics. Hahlin *et al.*,[33] who implemented the same method of sample preparation as used in the present work, concluded that water does not contaminate ex-situ prepared electrodes. Lyon *et al.*[34] considered contamination by organic materials, and argued that such impurities introduce only weak interface dipoles and their effect is insignificant. In accordance with literature, we find no evidence of contamination effects in the present experiment.

Time-resolved photoemission spectrometer

A detailed description and characterization of the XUV light source can be found elsewhere.[30] Briefly, a Ti:sapphire laser system delivering 2.5 mJ, 800 nm, 25 fs pulses at a repetition rate of 5 kHz was used to generate the visible pump and the XUV probe beams. The laser output

was split so that approximately 1.5 mJ pulse energy was used for the frequency up-conversion via the HHG process in an argon-filled cell to generate XUV pulses. The 21st harmonic of the fundamental frequency, with a photon energy of 32 eV, was selected with the use of a reflective off-center zone plate and refocused by a toroidal mirror into the experimental chamber. The XUV photon flux in the interaction region was $\sim 10^6$ photons per pulse, as measured by means of a calibrated photo diode. Another part of the laser output was used for pumping of an optical parametric amplifier (OPA) to generate pulses at 530 nm wavelength. The spot sizes of the pump and the probe beams at the sample were 500 μm and 100 μm, respectively. The pump pulse energy was 4 μJ, corresponding to a photon flux of 5×10^{15} photons/cm^2 in the interaction region. A computer-controlled delay stage was used in the pump beam path to vary the time delay between the pump and probe pulses. A time resolution of 98 fs (FWHM) in the present experiment was inferred from a cross correlation measurement carried out on the bTiO_2 sample, as we discuss in detail below.

The kinetic energy spectra of photoelectrons were measured with the use of a time-of-flight (TOF) electron spectrometer THEMIS 600 delivered by SPECS. The spectrometer is equipped with a cylindrical multi-element electrostatic lens that maps electrons emitted from the sample onto a detector positioned at the end of the drift region. The lens can be operated in different modes, differing in the electron acceptance angle, the spectral energy range, and the energy resolution. In the drift mode (DM), the electrostatic lens is disabled and the spectrometer performs as a classical drift tube with an acceptance angle of $\pm 1^\circ$, determined by the ratio of the detector aperture and the spectrometer length. This mode was used to acquire steady-state photoelectron spectra in a wide kinetic energy range. The wide-angle mode (WAM) yields the highest acceptance angle of $\pm 15^\circ$, though the kinetic energy scale is limited to a certain range around a predefined kinetic energy. This mode was used for acquisition of spectra with a high signal-to-noise ratio in an energy range sufficient to reveal the spectral components of XUV ionization from the ground state of the N719 dye and from the transient states. To avoid saturation of the detector, the electron count

rate was maintained below the pulse repetition rate of the laser system. Since the XUV ionization yield per pulse is rather high, the detector was equipped with a low-energy filter which did not pass electrons with kinetic energies below a chosen value. This was achieved by applying a deceleration voltage to a grid positioned in front of the detector. The calibration of the spectrometer's work function was carried out by measuring the Fermi edge of a gold sample. The binding energies reported in this work are obtained from the measured electron kinetic energies with the work function taken into account. The spectral energy resolution was mainly determined by the HHG bandwidth convoluted with the spectrometer resolution. An energy resolution of 0.1 eV was derived from a calibration measurement by recording a XUV ionization spectrum of argon gas.

Results and Discussion

Steady-state XUV spectra

The energy structure of the ground state of N719 and the valance band of TiO_2 are inferred from steady-state XUV spectra, recorded without application of the pump beam. Fig. 1 shows the results obtained for the bare and sensitized TiO_2 films. The spectra were recorded with equal acquisition times. The positions of the higher-lying energy levels are important for the photoinduced electron transfer at the N719/TiO_2 interface, and can be elucidated from these measurements. The valence-band edge of the non-sensitized TiO_2 sample lies at a binding energy of 3.2 eV.[35,36] This value was obtained by fitting a line to the spectral onset and using the intersection point of this line with the abcissa axis. From the analysis of the absorption spectrum measured for bTiO_2, we obtained a value of 3.3 eV for the energy gap between the valence and conduction bands. Using this value the conduction band edge position can be estimated to lie 0.1 eV above the Fermi edge.[34] For the sensitized sample, the maximum of the HOMO band of the N719 dye arises at a binding energy of $\sim$ 2.2 eV. This value is in agreement with previously reported results for the N719/TiO_2 interface.[34] At

binding energies larger than 4 eV, photoemission from the valence band of TiO_2 dominates the ionization yield. In this energy range the signal intensity of $bTiO_2$ is higher (see Fig. 1). This is due to the fact that, for the sensitized sample, the dye absorbs XUV light as well as attenuates electrons emitted from the substrate.

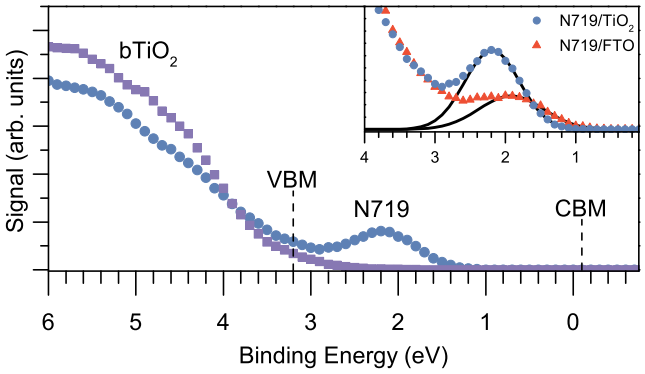

Figure 1: (Color online) Steady-state XUV spectra of photoelectrons recorded for the bare (squares) and sensitized (circles) TiO_2 samples. The emission peak from the ground state of the dye is labeled by N719. The inset shows a comparison of emission spectra obtained for sensitized TiO_2 (circles) and FTO (triangles) samples. The solid lines show the fit results of the HOMO ionization signal to a Gaussian profile.

The inset of Fig. 1 shows a comparison of XUV spectra of the sensitized TiO_2 and FTO electrodes. For both samples, the ionization contribution from the HOMO band was fitted to a Gaussian profile in the region of lower binding energies where contribution from the valence band of the substrate can be disregarded. One can see that the HOMO-band contribution for the TiO_2 electrode appears stronger and its peak position lies 0.3 eV higher on the energy scale. The latter manifests the difference in the electronic coupling between the dye and the two surfaces. One should note that the character of the dye-surface interaction affects not only the energetic structure at the interfaces but also the electron kinetics at higher excitation level, as we discuss below. The difference in the ionization yield from the HOMO band can be easily understood as being due to different surface roughnesses of the two electrodes, leading to a different amount of dye deposited on the surface. This is an important issue here, since the FTO substrate is used as a reference and the transient signal needs to be normalized to the amount of deposited dye. From the results shown in Fig. 1,

we find that the colloidal TiO_2 surface maintains by a factor of 2.4 higher amount of dye than the FTO surface. This was obtained by comparing the HOMO-band yields integrated over the respective Gaussian profiles.

Pump-probe measurements with $bTiO_2$ and bFTO: spectrometer resolution

Before considering the injection kinetics at the dye–semiconductor interface, it is instructive to present results of pump-probe measurements with the use of bare $bTiO_2$ and bFTO samples. These measurements facilitated to reveal possible contributions from the substrates to the transient signal of the sensitized samples as well as to determine the time resolution achieved in the experiment. When the pump and the probe pulses overlap in time, a process of multiphoton ionization occurs that involves absorption of an XUV probe photon simultaneously with absorption or emission of one or more pump photons. This process does not require the presence of an excited state that can be resonantly populated by the pump beam. It has received a description in terms of laser-assisted photoelectric effect from a surface.[37,38] The ionization yield integrated over a sideband of the laser-assisted ionization process represents a cross correlation (CC) signal of the pump and the probe beams. By recording the CC signal at higher kinetic energies in the XUV emission spectrum as a function of the time delay, we obtained a CC trace representing a convolution of temporal profiles of the pump and the probe pulses.

The results recorded with the $bTiO_2$ sample are presented in Fig. 2 (see left panel). A fit of experimental data to a Gaussian profile yields a CC width of 98 fs (FWHM). This value constitutes the time resolution in the pump-probe measurements. The right panels in Fig. 2 demonstrate the appearance of the laser-assisted ionization sideband in the kinetic energy spectra. Here, the upper panel shows spectra recorded at time delays of 0 and $\pm$150 fs. Their difference (see the lower panel) reveals the CC signal. The CC measurements also enabled to define the delay stage position at which the pump and probe pulses overlapped in time in

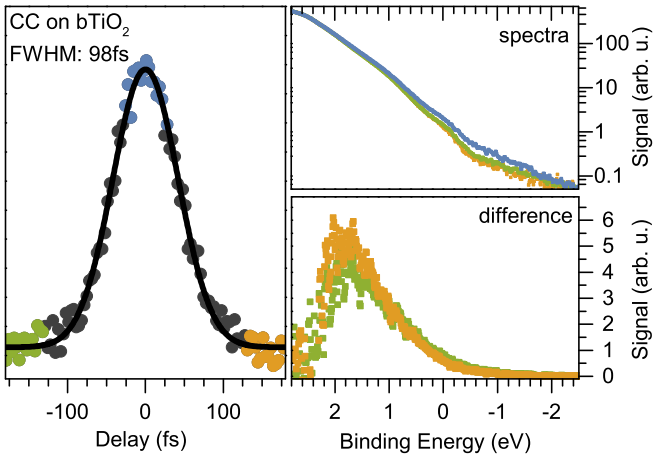

Figure 2: (Color online) CC measurements performed with the bare TiO_2 sample. Left panel: the transient background-subtracted signal, the solid curve shows the fit of the CC trace to a Gaussian profile. Top right panel: electron energy spectra recorded at −150 fs (green), 0 fs (blue), and +150 fs (yellow) time delays. Bottom right panel: difference between the spectra obtained at zero and −150 fs (green) or +150 fs (yellow) time delays.

the interaction region. It is important to note that XUV spectra recorded at a given positive or negative time delay of the same absolute value are identical. This means that the pump beam does not initiate electron population dynamics in the bare samples and laser-assisted ionization is the only process where it plays a role. Very similar results were obtained for the bFTO sample.

The peak intensity of the pump pulse was attenuated down to $\sim 10^{10}$ W/cm^2 to prevent excessive ionization of the sample by this beam. At such an intensity, only a small amount of slow electrons was generated by the pump pulse and their contribution to the higher-energy part of the XUV spectrum was negligible. The spectral shift due to the spatial charge effect[39] was also negligibly small. This was verified by comparing the pump-probe spectra recorded at negative time delays (the probe pulse arrives first to the interaction region) with the steady-state XUV spectra. The negative-delay pump-probe spectra are, thus, used as a background measurement in the analysis of transient spectra presented below.

Ultrafast kinetics on dye-sensitized samples

The injection kinetics in the dye-sensitized samples was studied at the same experimental conditions as described above. Fig. 3 shows the transient signal recorded for the N719/TiO_2 and N719/FTO interfaces, respectively. The signal represents an electron yield integrated in the background-subtracted XUV spectra over the range of binding energies between 1 eV and -2 eV. This range lies above the HOMO band of N719 and encompasses the ionization contributions from transient states excited by the pump beam. Pump-probe spectra for negative time delays were used as a background measurement. Both transients were obtained with identical integration time and pump intensity and were not normalized. There is a dramatic difference in the electron population dynamics of the sensitized samples as compared to the CC trace of bare samples, which is also reproduced in Fig. 3 by the gray line. Except for short time delays in the vicinity of time zero, where the finite time resolution prescribes the Gaussian shape of the transient signal, both curves in Fig. 3 exhibit a multicomponent exponential decay. This decay, however, is different for the two samples, which enables us to identify the unique properties of the electron transfer at the N719/TiO_2 interface.

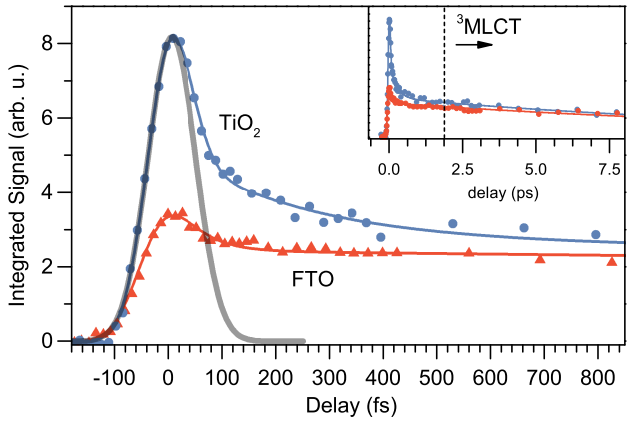

Figure 3: (Color online) Transient XUV ionization signal from sensitized TiO_2 (circles) and FTO (triangles) samples. The inset shows the transient signal in a larger range of time delays. The vertical line indicates a time delay beyond which the transient signal is dominated by ionization from the ^{3}MLCT state. The solid lines represent fits to the transient signals. (see section:Injection kinetics)

The main difference arises on the early time scale below $\sim$ 2 ps, where the two transient

dependencies exhibit a fast decay but clearly deviate from each other. At time delays larger than 2 ps, both transients manifest similar slow decay that occurs on a time scale of several picoseconds (see the inset in Fig. 3 for a larger delay range). In order to identify different decay channels and to determine the binding energies of the involved transient states, we consider separately the XUV spectra measured for the two distinct time domains: at time zero and at time delays larger than 2 ps. These spectra are shown in Figs. 4(a) and (b), respectively.

The long-lived species appears to have the same binding energy and decay rate for both sensitized samples. Therefore, we assign this spectral component to population of the thermally relaxed ^{3}MLCT state of the dye. This is in accordance with the known fact that the triplet state manifests similar injection kinetics at different interfaces.[12,40] Its binding energy of 0.1 eV and a width of 0.8 eV were obtained from a fit of the energy peak to a Gaussian profile (see Fig. 4(b)). The specified width represents a result of deconvolution of the apparatus energy resolution from the fit value. It follows that the ^{3}MLCT state lies 0.2 eV below the conduction band minimum. Injection from this state, however, is possible due to its large bandwidth, resulting in a partial energy overlap with the conduction band.

In order to reveal in more detail any differences in the early-time dynamics at the N719/TiO_2 and the N719/FTO interfaces, the slow-decaying ^{3}MLCT energy peak was subtracted from the spectra recorded at time zero. The results of subtraction are shown in Fig. 4(c). One can see that the residual signal for the FTO sample is much smaller than for the TiO_2 sample, much more important the structure of the residual spectrum is different for the two electrodes. Whereas for the FTO electrode the residual signal consists of a single energy peak centered at a binding energy of -0.8 eV, a superposition of two peaks is apparent in the TiO_2 residual spectrum. This was inferred from a fit of experimental data to a sum of two Gaussian profiles. One of the peaks contributing to the TiO_2 spectrum lies at the same binding energy of -0.8 eV as the single peak of the N719/FTO residual spectrum. For both electrodes, the lifetime of this spectral component is nearly the same

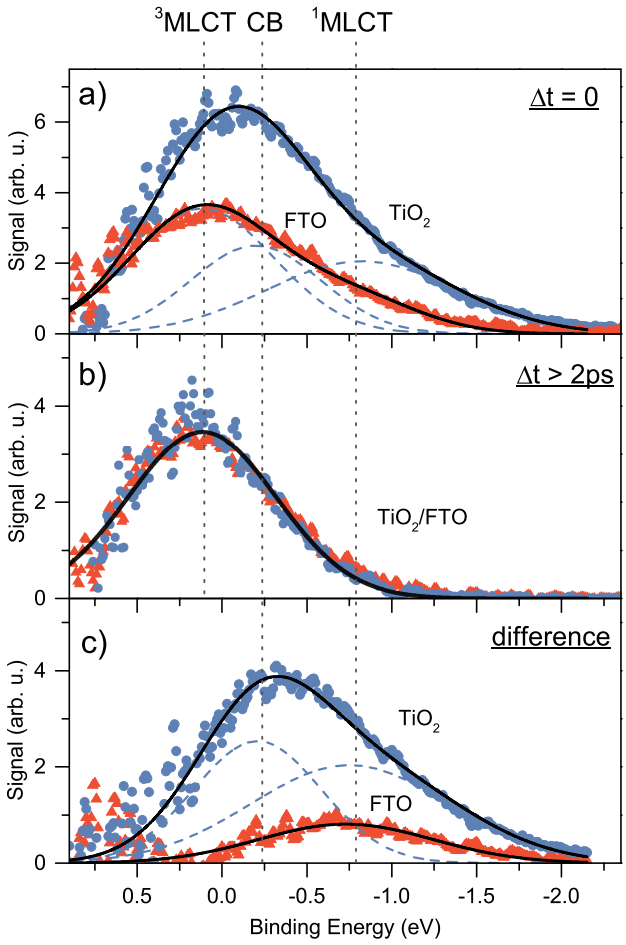

Figure 4: (Color online) Transient energy spectra of photoelectrons emitted from sensitized TiO_2 (circles) and FTO (triangles) samples at (a) zero time delay and (b) at time delays larger than 2 ps. The panel (c) shows the difference between spectra in (a) and (b). Vertical lines indicate positions of the energy peaks attributed to ionization of the ^{1}MLCT, ^{3}MLCT, and CB states. The individual contributions from the ^{1}MLCT and CB states to the TiO_2 spectrum are shown by dashed lines. Solid lines show results of superposition of the corresponding number of energy peaks: ^{1}MLCT, ^{3}MLCT, and CB peaks in (a); ^{3}MLCT peak in (b); ^{1}MLCT and CB peaks in (c).

as the CC width (see discussion below). It is therefore attributed to the short-lived ^{1}MLCT state directly populated by the pump beam. Another peak contributing to the N719/TiO_2 residual spectrum lies at a binding energy of -0.2 eV. It arises only in the spectra recorded for the sensitized TiO_2 electrode and, thus, manifests the specific interaction between the dye and the CB of semiconductor. Hence, we denote this peak by CB of TiO_2.

Since the CB peak is not apparent for the FTO electrode, we conclude that the ^{1}MLCT$\rightarrow$CB

injection is weak and can be neglected. The weakness of this transition is a consequence of the specific electronic coupling at the N719/FTO interface. This is in accordance with the results of previous studies, where electron injection was found to be much slower for nano-colloidal SnO_2 compared to TiO_2 [31,32,41] It was argued that a possible reason could be the much lower density of acceptor states of the FTO conduction band resulting in a smaller probability for the electron transfer process. Considering the competing ultrafast relaxation channel to the triplet state the total yield of electrons injected from the ^{1}MLCT state, is therefore highly suppressed.

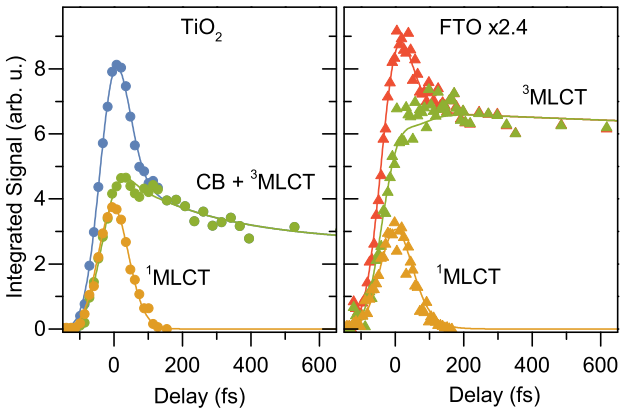

Figure 5: (Color online) Spectral decomposition of the transient signal shown in Fig. 3. Left panel: TiO_2 signal is decomposed into the ^{1}MLCT contribution (yellow) and the combined contribution of ^{3}MLCT and CB states (green). Right panel: FTO signal is decomposed into the ^{1}MLCT (yellow) and ^{3}MLCT (green) contributions. The FTO signal is multiplied by the factor 2.4 to account for the different surface coverage. The solid lines represent fits to the transient signals. (see section:Injection kinetics)

Our measurement indicate that the energy level of the ^{1}MLCT state lies 0.7 eV above the conduction band edge. Such a driving force is preferable for ultrafast injection.

It is important to note that although we apply a pump photon energy of 2.3 eV, the energy difference between the center of the HOMO band and the ^{1}MLCT state is found to be 3.0 eV. This means that the transition amplitude is larger for excitation on the higher-energy side of the HOMO band. This fact is illustrated in Fig. 6 where the initial state from which excitation takes place (denoted as ground state, GS) is depicted on the slope of the Gaussian profile representing the HOMO band. Therefore, it is questionable whether it is

possible to combine spectra obtained by means of PES and absorption spectroscopies, as it was carried out in Ref.[42] In that work, the absorption spectrum was shifted on the energy scale to match the difference between the absorption and emission peak positions with the photon energy.

The energy positions of the ^{1}MLCT, ^{3}MLCT, and CB peaks identified in Fig. 4 were found to be independent of the time delay. Therefore, for each time delay the transient spectra could be fitted to a sum of Gaussian profiles with fixed central energies. A sum of three and two profiles were used for fitting the TiO_2 and FTO data, respectively. Using this routine, we could decompose the integrated transient yield shown in Fig. 3 into its fast and slow individual components. The results of this decomposition are shown in Fig. 5 for the TiO_2 (left panel) and FTO (right panel) electrodes, respectively. Because of the small energy difference between the ^{3}MLCT and CB peaks for TiO_2, the fit could not provide reliable amplitudes of their individual contributions. Instead, the transient signal for the TiO_2 electrode was decomposed into a contribution of the ^{1}MLCT peak and a combined contribution of the ^{3}MLCT and CB peaks. For both electrodes, the transient ^{1}MLCT signal has almost the same shape as the CC trace. This means that the lifetime of the ^{1}MLCT state is smaller than the experimental temporal resolution of 98 fs. The transient ^{3}MLCT signal on the other hand exhibits a sharp increase at small time delays followed by a slow decay on a picosecond scale (see the decomposition results for the FTO electrode in the right panel of Fig. 5). However, the combined transient signal of ^{3}MLCT and CB of TiO_2 reveals an additional decay time constant. This decay, associated with the electron dynamics in the CB of TiO_2, is faster than the decay of the ^{3}MLCT state. This important issue is discussed in more detail below.

Injection kinetics

The results of the spectral decomposition of the transient signal were used to describe the electron dynamics at the dye–semiconductor interface and to derive the time constants of

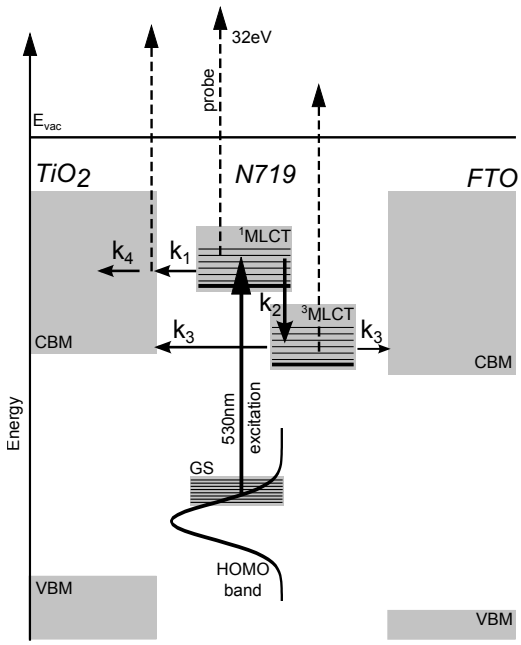

Figure 6: (Color online) Injection model for TiO_2 (left side) and FTO (right side). The vertical axis represents the energy scale. The energy positions of the ground (GS) and excited singlet and triplet MLCT states of the dye are shown together with the energy levels of the minimum CB energy (CBM) and the maximum valence band energy (VBM) for TiO_2 and FTO. The HOMO band of the dye is depicted by a Gaussian profile. The solid vertical arrow indicates the photoexcitation transition at 530 nm wavelength. Dashed arrows indicate XUV ionization transitions. $k_{1,2,3,4}$ denote rates of population and decay transitions considered in the model (see text).

involved electronic transitions. For this purpose, we have adapted the two-state injection model by Asbury *et al.*,[15,16] which is schematically depicted at the left side in Fig. 6. In this model, the initially populated non-thermalized ^{1}MLCT state can either inject electrons to TiO_2 with a rate k_1 or decay to the ^{3}MLCT state with a rate k_2. The decay rate k_2 is determined by intersystem crossing, followed by thermalization of the triplet state. A direct excitation of the ^{3}MLCT state from the ground state of dye was found to be improbable at the pump wavelength of 530 nm.[12] The ^{3}MLCT state can inject electrons to TiO_2 with a rate k_3. In the transient spectra, however, the spectral component associated with electrons injected to the CB from the triplet state is not distinguished. Therefore, in our analysis only

the transient yield of injection from the singlet state, derived from the spectral decomposition procedure, is considered. The recombination to the ground state of the dye was reported to occur on a microsecond to millisecond time scale.[43] Since this is a by orders of magnitudes slower process compared to the injection channels, we disregard it in our consideration. Dissipation of the injected electrons is described by a rate constant k_4. The origin of this decay will be discussed below. The electron dynamics at the N719/FTO interface (see the right side of Fig. 6) are treated in a similar fashion, except that we do not consider the ^{1}MLCT$\rightarrow$CB transition as discussed above.

The electron population dynamics at the N719/TiO_2 interface can be described by the system of differential equations:

$$\begin{aligned} \dot{n}_{\mathrm{S}} &= -(k_1 + k_2) n_{\mathrm{S}} + P(t) \ , \\ \dot{n}_{\mathrm{T}} &= k_2 n_{\mathrm{S}} - k_3 n_{\mathrm{T}}, \\ \dot{n}_{\mathrm{CB}} &= k_1 n_{\mathrm{S}} - k_4 n_{\mathrm{CB}} \quad , \end{aligned} \tag{1}$$

where $n_{\mathrm{S,T,CB}}$ denote the populations of the ^{1}MLCT, ^{3}MLCT, and CB states, respectively, and $P(t)$ describes the time-dependent population rate of the ^{1}MLCT state with the actual temporal envelope of the pump pulse taken into account. One should stress again that n_{CB} describes the CB state populated via injection from the ^{1}MLCT state and, thus, the rate constant k_3 is not involved in the third line of Eq. (1).

It is instructive to consider first the solution of Eq. (1) in the limit of long time delays, $t \gg \tau_{\mathrm{CC}}$, where the population $n_{\mathrm{T}}(t)$ of the triplet ^{3}MLCT state constitutes the transient signal. Here τ_{CC} represents the CC width. In this limit, the term $P(t)$ becomes negligibly small and the solution for $n_{\mathrm{T}}(t)$ can be found analytically. Taking into account that $k_3 \ll k_1, k_2$, we obtain

$$n\,(t) \propto \frac{k_2}{k_1 + k_2 - k_3} \exp\left(-k_3 t\right) \ . \tag{2}$$

The same equation describes the population dynamics of the ^{3}MLCT state at the N719/FTO

interface in the limit of long time delays. In this case the rate k_1 should be neglected, $k_1 = 0$, since injection from the ^{1}MLCT state to FTO is excluded. One should note again that the decay rate k_3 of the ^{3}MLCT state is found to be the same for both TiO_2 and FTO electrodes. It means that in the asymptotic time limit the ratio of populations of the triplet state at the two interfaces is constant, $n_{\mathrm{T,FTO}}(t)/n_{\mathrm{T,TiO_2}}(t) = A$ $(t \to +\infty)$. Using the inequality $k_3 \ll k_1, k_2$, from Eq. (2) we derive

$$\frac{k_1}{k_2} = A - 1 \ . \tag{3}$$

For the value $A = 2.4$ obtained from the experimental data (see section:Steady-state XUV spectra), we find that the ratio of the competing injection and relaxation rates of the ^{1}MLCT state at the N719/TiO_2 interface is $k_1/k_2 = 1.4$. Thus, the injection rate into the CB is higher than the decay rate. Our finding is in a good agreement with the previously reported ratio of 1.5.[17] This supports the approximation made in our model, where we neglected the injection channel from the ^{1}MLCT state into FTO.

At shorter time delays, the temporal envelopes of the pump and probe pulses need to be taken into account to reproduce the experimental results. In this case the system of rate equations in Eq. (1) was solved numerically with the initial condition that all involved states were unpopulated at $t \to -\infty$. The ionization signal from the ^{1}MLCT, ^{3}MLCT and CB states was calculated by convolution of $n_{\mathrm{S}}(t)$, $n_{\mathrm{T}}(t)$ and $n_{\mathrm{CB}}(t)$ with the temporal envelope of the probe pulse, assuming that the probe step is non-saturated. A Gaussian envelope was assumed for both pump and probe pulses, with a constrain that their convolution yields the measured CC trace. The numerical results were fitted to the spectrally decomposed experimental data shown in Fig. 5, with rates $k_{1,2,3,4}$ being as fit parameters. The fit routine was applied to reproduce simultaneously the data sets obtained for both electrodes. In order to account for the CC signal from the bare substrates, a CC trace centered at time zero was added to the fit function and its amplitude was considered as an independent fit parameter.

Table 1: Population (τ_p) and decay (τ_d) time constants of the ^{1}MLCT, ^{3}MLCT, and CB states obtained from the modeling of the electron dynamics with the use of Eq. (1). The values obtained in the present work are given in comparison with previously reported results. The binding energies (E_b) of the states and their widths (ΔE_b) are also presented.

State	E_b (eV)	ΔE_b(eV)	τ_p	τ_d
^{1}MLCT	-0.8	1.0	–	(20 ± 10) fs
			–	30 fs[17]
			–	(30 ± 3) fs[16]
CB	-0.2	0.6	(50 ± 20) fs	(250 ± 30) fs
			(50 ± 6) fs[17]	–
			< 100 fs[15]	–
^{3}MLCT	0.1	0.8	(30 ± 20) fs	(15 ± 2) ps
			(75 ± 10) fs[17]	–
			(80 ± 5) fs[16]	–
			< 100 fs[15]	–
HOMO band	2.2	0.6	–	–

Table I summarizes the results obtained from the simulation of the population and relaxation electron dynamics at the N719/TiO_2 and N719/FTO interfaces. Here the population and the decay time constants represent inverse values of the corresponding transition rates, except for the decay of the ^{1}MLCT state the time constant is represented by $1/(k_1 + k_2)$. The rather large error bars of the ^{3}MLCT and CB population time constants are due to the limited time resolution in experiment. It prevents derivation of a convincing value of k_1/k_2 from the early-time dynamics simulation. The τ_p value of 50 fs obtained for the ^{1}MLCT$\rightarrow$CB transition is in a good agreement with the previously reported results,[15,17] though the population rate of the triplet state seems to be overestimated in the simulation. This is most probably due to the presence of the CC signal in the transient spectra which spectrally overlaps with the signal from the triplet state. The ^{1}MLCT state lifetime of 20$\pm$10 fs could also be derived by considering the minor broadening of the spectrally separated ^{1}MLCT component (see Fig. 5) as compared to the CC trace. This lifetime is in agreement with the literature value of 30 fs.[15,17] The injection rate k_3 is found to yield the lifetime of 15 ps for the ^{3}MLCT state at both interfaces. In a previous investigation focusing on the injection

kinetics from the ^{3}MLCT state it was shown that injection takes place on equal time scales at both interfaces and is controlled by a similar electronic coupling mechanism.[12] Multiexponential kinetics were measured ranging from several ps up to 100ps and are in agreement with our findings.[12,16] The ultrafast populated CB peak exhibits a decay constant of the order of 250 fs. Since this signal is due to electrons located at the semiconductor site, the decay mechanism needs to be related to the CB properties. To date, results of studies on the carrier relaxation dynamics in TiO_2 are sparsely presented in literature. By using the method of transient absorption spectroscopy, Tamaki *et al.*[44] reported on the capture of free electrons into trap states at the semiconductor surface, occurring on a time scale of $\sim$ 200 fs. Such a dissipation mechanism could be particularly efficient in the present experiment due to the enlarged surface area of the substrate. A similar decay time constant of 300 fs was inferred from the measurements of carrier mobility with the use of time-resolved terahertz spectroscopy.[45] An alternative dissipation mechanism could be the electron escape from the probed surface into the bulk. Indeed, photoelectron spectroscopy allows probing the electron population within a surface skin layer of a few Å thickness, and the escape mechanism could well describe our observations. The kinetics of electron escape from surface was considered by Gundlach *et al.*,[46] who applied time-resolved photoemission spectroscopy with a 10 fs time resolution to study charge transfer dynamics between catechol molecules adsorbed on a rutile TiO_2 substrate. It was found that the escape kinetics is characterized by an initial time constant below 10 fs, followed by a slower escape on a time scale of 50–100-fs and, eventually, by a long-lived tail in a picosecond range. One should also note that the electron motion direction with respect to the surface plays an important role in the escape kinetics, as reported by Rego *et al.*[47] on the basis of quantum-dynamics calculations. It was predicted that an injected electron diffuses into the [101] bulk direction on a 100 fs time scale. Considering the random surface orientation of nano-colloidal particles used as the substrate in the present experiment, we find a good match between this value and the reported here time constant of the CB signal decay.

Summary

We have demonstrated that transient XUV photoemission spectroscopy is advantageous in revealing simultaneously both the injection kinetics at a dye–semiconductor interface and the energy structure of this complex system. With the use of this method, we identified for the first time directly the absolute binding energies of the singlet and triplet excited MLCT states of the N719 dye which are involved in the electron dynamics following the photoexcitation event. The singlet state is found to lie at 0.7 eV above the conduction band minimum, which gives rise to a strong force for injection from this state. The triplet state lies 0.2 eV *below* the conduction band. Injection from the triplet state, thus, occurs due to a partial energy overlap with the conduction band, leading to a slow kinetics of the electron transfer. It is important to note that the energy difference between the center of the HOMO band and the center of the ^{1}MLCT band is 3.0 eV, which is by 0.7 eV larger than the photon energy at the absorption maximum of the dye. The spectral decomposition of the transient emission signal allows the ultrafast population and decay dynamics of the excited states to be followed individually. For the N719/TiO_2 interface, contributions from the directly excited ^{1}MLCT state, the CB state of injected electrons, and the thermally relaxed ^{3}MLCT state were identified. By comparing results obtained for the N719/TiO_2 and N719/FTO interfaces, we could unambiguously reveal the kinetics of injected electrons at the CB site. The ultrafast injection to TiO_2 was confirmed to occur from the non-thermalized ^{1}MLCT state, whereas the injection yield from this state was found to be negligible for the FTO electrode. The time constants of the population and decay dynamics inferred in this study are in a good agreement with the values reported in literature. Considering the dissipation of injected electrons at the CB site, both the electron trapping and the electron escape models could interpret our observations. Further investigations are needed to determine the probable dissipation mechanism.

Acknowledgement

This work is funded by the European Research Council, Grant No. 279344 (E.F.A.), and by the Helmholtz-Gemeinschaft via the VH-NG-635 Grant (E.F.A.). L. Spiccia gratefully acknowledges funding from the Australian Research Council through the ARC Centre of Excellence for Electromaterials Science (ACES)

References

(1) Ardo, S.; Meyer, G. J. Photodriven Heterogeneous Charge Transfer with Transition-Metal Compounds Anchored to TiO_2 Semiconductor Surfaces. *Chem. Soc. Rev.* **2009**, *38*, 115–164.

(2) O'Regan, B.; Grätzel, M. A Low-Cost, High-Efficiency Solar Cell Based on Dye-Sensitized Colloidal TiO_2 Films. *Nature* **1991**, *353*, 737–740.

(3) Nazeeruddin, M. K.; Kay, A.; Rodicio, I.; Humphry-Baker, R.; Mueller, E.; Liska, P.; Vlachopoulos, N.; Grätzel, M. Conversion of Light to Electricity by Cis-X2bis(2,2'-bipyridyl-4,4'-dicarboxylate)Ruthenium(II) Charge-Transfer Sensitizers (X = Cl-, Br-, I-, CN-, and SCN-) on Nanocrystalline Titanium Dioxide Electrodes. *J. Am. Chem. Soc.* **1993**, *115*, 6382–6390.

(4) Nazeeruddin, M. K.; Zakeeruddin, S. M.; Humphry-Baker, R.; Jirousek, M.; Liska, P.; Vlachopoulos, N.; Shklover, V.; Fischer, C.-H.; Grätzel, M. Acid-Base Equilibria of (2,2-Bipyridyl-4,4-dicarboxylic acid)ruthenium(II) Complexes and the Effect of Protonation on Charge-Transfer Sensitization of Nanocrystalline Titania. *Inorg. Chem.* **1999**, *38*, 6298–6305.

(5) Grätzel, M. Recent Advances in Sensitized Mesoscopic Solar Cells. *Acc. Chem. Res.* **2009**, *42*, 1788–1798.

(6) Hagfeldt, A.; Boschloo, G.; Sun, L.; Kloo, L.; Pettersson, H. Dye-Sensitized Solar Cells. *Chem. Rev.* **2010**, *110*, 6595–6663.

(7) Tachibana, Y.; Moser, J. E.; Grätzel, M.; Klug, D. R.; Durrant, J. R. Subpicosecond Interfacial Charge Separation in Dye-Sensitized Nanocrystalline Titanium Dioxide Films. *J. Phys. Chem.* **1996**, *100*, 20056–20062.

(8) Hannappel, T.; Burfeindt, B.; Storck, W.; Willig, F. Measurement of Ultrafast Photoinduced Electron Transfer from Chemically Anchored Ru-Dye Molecules into Empty Electronic States in a Colloidal Anatase TiO_2 Film. *J. Phys. Chem. B* **1997**, *101*, 6799–6802.

(9) Tachibana, Y.; Nazeeruddin, M. K.; Grätzel, M.; Klug, D. R.; Durrant, J. R. Electron Injection Kinetics for the Nanocrystalline TiO_2 Films Sensitised with the Dye $(Bu_4N)_2Ru(dcbpyH)_2(NCS)_2$. *Chem. Phys.* **2002**, *285*, 127–132.

(10) Anderson, N. A.; Lian, T. Ultrafast Electron Transfer at the Molecule-Semiconductor Nanoparticle Interface. *Annu. Rev. Phys. Chem.* **2005**, *56*, 491–519.

(11) Ramakrishna, G.; Jose, D. A.; Kumar, D. K.; Das, A.; Palit, D. K.; Ghosh, H. N. Strongly Coupled Ruthenium-Polypyridyl Complexes for Efficient Electron Injection in Dye-Sensitized Semiconductor Nanoparticles. *J. Phys. Chem. B* **2005**, *109*, 15445–15453.

(12) Myllyperkiö, P.; Benkö, G.; Korppi-Tommola, J.; Yartsev, A. P.; Sundström, V. A Study of Electron Transfer in $Ru(dcbpy)_2(NCS)_2$ Sensitized Nanocrystalline TiO_2 And SnO_2 Films Induced by Red-Wing Excitation. *Phys. Chem. Chem. Phys.* **2008**, *10*, 996–1002.

(13) Asbury, J. B.; Ellingson, R. J.; Ghosh, H. N.; Ferrere, S.; Nozik, A. J.; Lian, T. Femtosecond IR Study of Excited-State Relaxation and Electron-Injection Dynamics of

$Ru(dcbpy)_2(NCS)_2$ in Solution and on Nanocrystalline TiO_2 and Al_2O_3 Thin Films. *J. Phys. Chem. B* **1999**, *103*, 3110–3119.

(14) Asbury, J. B.; Wang, Y.-Q.; Hao, E.; Ghosh, H. N.; Lian, T. Evidences of Hot Excited State Electron Injection from Sensitizer Molecules to TiO_2 Nanocrystalline Thin Films. *Res. Chem. Intermed.* **2001**, *27*, 393–406.

(15) Asbury, J. B.; Anderson, N. A.; Hao, E.; Ai, X.; Lian, T. Parameters Affecting Electron Injection Dynamics from Ruthenium Dyes to Titanium Dioxide Nanocrystalline Thin Film. *J. Phys. Chem. B* **2003**, *107*, 7376–7386.

(16) Benkö, G.; Kallioinen, J.; Korppi-Tommola, J. E. I.; Yartsev, A. P.; Sundström, V. Photoinduced Ultrafast Dye-to-Semiconductor Electron Injection from Nonthermalized and Thermalized Donor States. *J. Am. Chem. Soc.* **2002**, *124*, 489–493.

(17) Kallioinen, J.; Benkö, G.; Sundström, V.; Korppi-Tommola, J. E. I.; Yartsev, A. P. Electron Transfer from the Singlet and Triplet Excited States of $Ru(dcbpy)_2(NCS)_2$ into Nanocrystalline TiO_2 Thin Films. *J. Phys. Chem. B* **2002**, *106*, 4396–4404.

(18) Gerischer, H. Charge Transfer Processes at Semiconductor-Electrolyte Interfaces in Connection with Problems of Catalysis. *Surf. Sci.* **1969**, *18*, 97–122.

(19) Liu, G.; Klein, A.; Thissen, A.; Jaegermann, W. Electronic Properties and Interface Characterization of Phthalocyanine and Ru-polypyridine Dyes on TiO_2 Surface. *Surf. Sci.* **2003**, *539*, 37–48.

(20) Snook, J. H.; Samuelson, L. A.; Kumar, J.; Kim, Y.-G.; Whitten, J. E. Ultraviolet Photoelectron Spectroscopy of Nanocrystalline TiO_2 Films Sensitized with (2,2-bipyridyl)ruthenium(II) Dyes for Photovoltaic Applications. *Org. Electron.* **2005**, *6*, 55–64.

(21) Lenzmann, F.; Krueger, J.; Burnside, S.; Brooks, K.; Grätzel, M.; Gal, D.; Rühle, S.; Cahen, D. Surface Photovoltage Spectroscopy of Dye-Sensitized Solar Cells with TiO_2, Nb_2O_5, and $SrTiO_3$ Nanocrystalline Photoanodes: Indication for Electron Injection from Higher Excited Dye States. *J. Phys. Chem. B* **2001**, *105*, 6347–6352.

(22) Angelis, F. D.; Fantacci, S.; Selloni, A. Alignment of the Dye's Molecular Levels with the TiO_2 Band Edges in Dye-Sensitized Solar Cells: A DFT-TDDFT Study. *Nanotechnology* **2008**, *19*, 424002.

(23) De Angelis, F.; Fantacci, S.; Mosconi, E.; Nazeeruddin, M. K.; Grätzel, M. Absorption Spectra and Excited State Energy Levels of the N719 Dye on TiO_2 in Dye-Sensitized Solar Cell Models. *J. Phys. Chem. C* **2011**, *115*, 8825–8831.

(24) Li, X. F.; L'Huillier, A.; Ferray, M.; Lompr, L. A.; Mainfray, G. Multiple-Harmonic Generation in Rare Gases at High Laser Intensity. *Phys. Rev. A: At., Mol., Opt. Phys.* **1989**, *39*, 5751–5761.

(25) Brabec, T.; Krausz, F. Intense Few-Cycle Laser Fields: Frontiers of Nonlinear Optics. *Rev. Mod. Phys.* **2000**, *72*, 545–591.

(26) Siefermann, K. R.; Liu, Y.; Lugovoy, E.; Link, O.; Faubel, M.; Buck, U.; Winter, B.; Abel, B. Binding Energies, Lifetimes and Implications of Bulk and Interface Solvated Electrons in Water. *Nature Chem.* **2010**, *2*, 274–279.

(27) Soifer, H.; Botheron, P.; Shafir, D.; Diner, A.; Raz, O.; Bruner, B. D.; Mairesse, Y.; Pons, B.; Dudovich, N. Near-Threshold High-Order Harmonic Spectroscopy with Aligned Molecules. *Phys. Rev. Lett.* **2010**, *105*, 143904.

(28) Nugent-Glandorf, L.; Scheer, M.; Samuels, D. A.; Mulhisen, A. M.; Grant, E. R.; Yang, X.; Bierbaum, V. M.; Leone, S. R. Ultrafast Time-Resolved Soft X-Ray Photoelectron Spectroscopy of Dissociating Br_2. *Phys. Rev. Lett.* **2001**, *87*, 193002.

(29) Billaud, P.; Géléoc, M.; Picard, Y. J.; Veyrinas, K.; Hergott, J. F.; Poullain, S. M.; Breger, P.; Ruchon, T.; Roulliay, M.; Delmotte, F. et al. Molecular Frame Photoemission in Dissociative Ionization Of H_2 And D_2 Induced by High Harmonic Generation Femtosecond XUV Pulses. *J. Phys. B: At., Mol. Opt. Phys.* **2012**, *45*, 194013.

(30) Metje, J.; Borgwardt, M.; Moguilevski, A.; Kothe, A.; Engel, N.; Wilke, M.; Al-Obaidi, R.; Tolksdorf, D.; Firsov, A.; Brzhezinskaya, M. et al. Monochromatization of Femtosecond XUV Light Pulses with the Use of Reflection Zone Plates. *Opt. Express* **2014**, *22*, 10747–10760.

(31) Asbury, J. B.; Hao, E.; Wang, Y.; Ghosh, H. N.; Lian, T. Ultrafast Electron Transfer Dynamics from Molecular Adsorbates to Semiconductor Nanocrystalline Thin Films. *J. Phys. Chem. B* **2001**, *105*, 4545–4557.

(32) Ai, X.; Anderson, N. A.; Guo, J.; Lian, T. Electron Injection Dynamics of Ru Polypyridyl Complexes on SnO_2 Nanocrystalline Thin Films. *J. Phys. Chem. B* **2005**, *109*, 7088–7094.

(33) Hahlin, M.; Johansson, E. M. J.; Schölin, R.; Siegbahn, H.; Rensmo, H. Influence of Water on the Electronic and Molecular Surface Structures of Ru-Dyes at Nanostructured TiO_2. *J. Phys. Chem. C* **2011**, *115*, 11996–12004.

(34) Lyon, J. E.; Rayan, M. K.; Beerbom, M. M.; Schlaf, R. Electronic Structure of the Indium Tin Oxide/Nanocrystalline Anatase (TiO_2)/Ruthenium-Dye Interfaces in Dye-Sensitized Solar Cells. *J. Appl. Phys.* **2008**, *104*, 073714.

(35) Xiong, G.; Shao, R.; Droubay, T. C.; Joly, A. G.; Beck, K. M.; Chambers, S. A.; Hess, W. P. Photoemission Electron Microscopy of TiO_2 Anatase Films Embedded with Rutile Nanocrystals. *Adv. Funct. Mater.* **2007**, *17*, 2133–2138.

(36) Lindblad, R.; Cappel, U. B.; O'Mahony, F. T. F.; Siegbahn, H.; Johansson, E. M. J.; Haque, S. A.; Rensmo, H. Energy Level Alignment in TiO_2/Metal Sulfide/Polymer

Interfaces for Solar Cell Applications. *Phys. Chem. Chem. Phys.* **2014**, *16*, 17099–17107.

(37) Miaja-Avila, L.; Lei, C.; Aeschlimann, M.; Gland, J. L.; Murnane, M. M.; Kapteyn, H. C.; Saathoff, G. Laser-Assisted Photoelectric Effect from Surfaces. *Phys. Rev. Lett.* **2006**, *97*, 113604.

(38) Saathoff, G.; Miaja-Avila, L.; Aeschlimann, M.; Murnane, M. M.; Kapteyn, H. C. Laser-Assisted Photoemission from Surfaces. *Phys. Rev. A: At., Mol., Opt. Phys.* **2008**, *77*, 022903.

(39) Oloff, L.-P.; Oura, M.; Rossnagel, K.; Chainani, A.; Matsunami, M.; Eguchi, R.; Kiss, T.; Nakatani, Y.; Yamaguchi, T.; Miyawaki, J. et al. Time-Resolved HAXPES at SACLA: Probe and Pump Pulse-Induced Space-Charge Effects. *New J. Phys.* **2014**, *16*, 123045.

(40) Benkö, G.; Myllyperkiö, P.; Pan, J.; Yartsev, A. P.; Sundström, V. Photoinduced Electron Injection from $Ru(dcbpy)_2(NCS)_2$ to SnO_2 and TiO_2 Nanocrystalline Films. *J. Am. Chem. Soc.* **2003**, *125*, 1118–1119.

(41) Furube, A.; Murai, M.; Watanabe, S.; Hara, K.; Katoh, R.; Tachiya, M. Near-IR Transient Absorption Study on Ultrafast Electron-Injection Dynamics from a Ru-Complex Dye into Nanocrystalline In_2O_3 Thin Films: Comparison with SnO_2, ZnO, and TiO_2 Films. *J. Photochem. Photobiol., A* **2006**, *182*, 273–279.

(42) Westermark, K.; Henningsson, A.; Rensmo, H.; Södergren, S.; Siegbahn, H.; Hagfeldt, A. Determination of the Electronic Density of States at a Nanostructured TiO_2/Ru-Dye/Electrolyte Interface by Means of Photoelectron Spectroscopy. *Chem. Phys.* **2002**, *285*, 157–165.

(43) Haque, S. A.; Tachibana, Y.; Klug, D. R.; Durrant, J. R. Charge Recombination Kinet-

ics in Dye-Sensitized Nanocrystalline Titanium Dioxide Films under Externally Applied Bias. *J. Phys. Chem. B* **1998**, *102*, 1745–1749.

(44) Tamaki, Y.; Furube, A.; Murai, M.; Hara, K.; Katoh, R.; Tachiya, M. Dynamics of Efficient Electron-Hole Separation in TiO_2 Nanoparticles Revealed by Femtosecond Transient Absorption Spectroscopy under the Weak-Excitation Condition. *Phys. Chem. Chem. Phys.* **2007**, *9*, 1453–1460.

(45) Turner, G. M.; Beard, M. C.; Schmuttenmaer, C. A. Carrier Localization and Cooling in Dye-Sensitized Nanocrystalline Titanium Dioxide. *J. Phys. Chem. B* **2002**, *106*, 11716–11719.

(46) Gundlach, L.; Ernstorfer, R.; Willig, F. Escape Dynamics of Photoexcited Electrons at Catechol : TiO_2(110). *Phys. Rev. B: Condens. Matter Mater. Phys.* **2006**, *74*, 035324.

(47) Rego, L. G. C.; Batista, V. S. Quantum Dynamics Simulations of Interfacial Electron Transfer in Sensitized TiO_2 Semiconductors. *J. Am. Chem. Soc.* **2003**, *125*, 7989–7997.

Graphical TOC Entry